第 43 卷第 1 期
2024 年 2 月

红 外 与 毫 米 波 学 报
J. Infrared Millim. Waves

Vol. 43，No. 1
February，2024

文章编号：1001−9014（2024）01−0063−07

DOI：10. 11972/j. issn. 1001−9014. 2024. 01. 009

Correlation between MBE deoxidation conditions and InGaAs/InP APD performance

GUO Zi-Lu[1,2,3]， WANG Wen-Juan[1,4*]， QU Hui-Dan[1]， FAN Liu--Yan[1]， ZHU Yi-Cheng[1,2]， WANG Ya-Jie[5]， ZHENG Chang-Lin[5]， WANG Xing-Jun[1]， CHEN Ping-Ping[1*]， LU Wei[1,2,3,4*]

（1. State Key Laboratory of Infrared Physics，Shanghai Institute of Technology Physics，Chinese Academy of Sciences，Shanghai 200083，China；
2. University of Chinese Academy of Sciences，Beijing 100049，China；
3. School of Physical Science and Technology，ShanghaiTech University，Shanghai 201210，China；
4. Shanghai Research Center for Quantum Sciences，Shanghai 201315，China；
5. State Key Laboratory of Surface Physics and Department of Physics，Fudan University，Shanghai 200438，China）

Abstract：InP-based InGaAs/InP avalanche photodiodes （APDs） have high sensitivity to near-infrared light，making them ideal optoelectronic devices for weak signal and single-photon detection. However，as device structures become complex and advanced，with thickness and sizes ranging from quantum dots to several micrometers，performance is increasingly constrained by defects in the lattice of the material and the process conditions. Solid source molecular beam epitaxy （MBE） technology was used to deoxidize InP substrates under the atmosphere As and P，respectively，and epitaxially grow lattice-matched $In_{0.53}Ga_{0.47}As$ film and InGaAs/InP avalanche APD full-structure materials. The experiment results demonstrate that As deoxidation has a distinct advantage over P deoxygenation in terms of MBE material quality，which can make a straight and sharp heterojunction interface，lower carrier concentrations，higher Hall mobilities，longer minority carrier lifetimes，and achieve suppression of dark current caused by point defects or impurity defects in the device. Therefore，As deoxidation can be applied effectively to enhance the quality of MBE materials. This work optimizes InP substrate InGaAs/InP epitaxial growth parameters and device fabrication conditions.

Key words：molecular beam epitaxy，P/As exchange，heterointerface diffusion，InGaAs/InP APD

MBE脱氧条件与InGaAs/InP APD性能的相关性

郭子路[1,2,3]， 王文娟[1,4*]， 曲会丹[1]， 范柳燕[1]， 诸毅诚[1,2]， 王亚杰[5]， 郑长林[5]， 王兴军[1]， 陈平平[1*]， 陆 卫[1,2,3,4*]

（1. 中国科学院上海技术物理研究所 红外物理国家重点实验室，上海 200083；
2. 中国科学院大学，北京 100049；
3. 上海科技大学 物质科学与技术学院，上海 201210；
4. 上海量子科学研究中心，上海 201315；
5. 复旦大学 应用表面物理国家重点实验室和物理学系，上海 200438）

摘要：InP基InGaAs/InP雪崩光电二极管（APD）对近红外光具有高敏感度，使其成为微弱信号和单光子探测的理想光电器件。然而随着先进器件结构越来越复杂，厚度尺寸从量子点到几微米不等，性能越来越受材料中晶格缺陷的影响和工艺条件的制约。采用固态源分子束外延（MBE）技术分别在As和P气氛保护下对InP衬

Received date：2023- 05- 05，**revised date**：2023- 09- 22　　　**收稿日期**：2023- 05- 05，**修回日期**：2023- 09- 22

Foundation items：Supported by the National Natural Science Foundation of China（12027805，62171136，62174166，and U2241219）；the Science and Technology Commission of Shanghai Municipality（Grant No. 2019SHZDZX01，22JC1402902）and the Strategic Priority Research Program of the Chinese Academy of Sciences（ XDB43010200）.

Biography：Guo Zilu（1992-），male，Baoding，China，Ph. D. candidate. Research area involves Semiconductor materials and devices. E-mail：guozl@shanghaitech. edu. cn.

[*] **Corresponding author**：E-mail：ppchen@mail. sitp. ac. cn，wangwj@mail. sitp. ac. cn，luwei@mail. sitp. ac. cn

底进行脱氧处理并外延生长晶格匹配的In0.53Ga0.47As薄膜和APD结构材料。实验结果表明,As脱氧在MBE材料质量方面比P脱氧具有明显的优势,可获得陡直明锐的异质结界面,降低载流子浓度,提高霍尔迁移率,延长少子寿命,并抑制器件中点缺陷或杂质缺陷引起的暗电流。因此,As脱氧可以有效提高MBE材料的质量,这项工作优化了InP衬底InGaAs/InP外延生长参数和器件制造条件。

关 键 词:分子束外延;P/As切换;异质界面扩散;铟镓砷/磷化铟雪崩光电二极管

中图分类号:O47 **文献标识码**:A

Introduction

The III-V semiconductor material InGaAs has a direct *band gap* and high *optical absorption efficiency* in the near-infrared band, which can be matched with the lattice of InP materials with good collisional ionization properties as one of the replaceable indirect *band gap* silicon-based materials[1]. Avalanche photodiodes (APDs) fabricated of InP and InGaAs materials for quantum key distribution[2], deep-space communications[3], 3-D light detection and ranging[4,5], etc., have many advantages such as high performance, high reliability, and low cost making a promising development outlook as optical signal detector applications. However, the performance of APDs is often limited by lattice defects in InP and InGaAs materials and the process conditions as the improvement of the structures. Therefore, preparing high-performance InGaAs/InP APD material remains challenging for researchers.

Molecular beam epitaxy (MBE) technology which has become more advanced in recent years, can control the parameters in the material deposition process, such as *temperature*, *gas flow rate*, sputtering, and deoxidation conditions, and precisely control the material *thickness* at the atomic layer scale, thus effectively regulating the material crystal structure and properties such as *mobility*, *dark current* and *light saturation current*[6,7]. In the MBE process, the atmosphere of evaporative sources is used to remove natural oxides from the substrate surface and protect against As evaporation damage, thus avoiding pollution from oxygen and other gases, known as deoxidation protection[8,9]. However, the effects of deoxidation atmospheres such as As and P sources on the performance of materials and devices, like impurities at arsenic-phosphorus heterojunctions, still need further research and optimization.[10,11].

In this paper, InP substrates were deoxidized under the atmosphere protection of As_4 and P_2, respectively. An ultra-high vacuum solid source molecular beam epitaxy (MBE) system grew lattice-matched $In_{0.53}Ga_{0.47}As$ film and APD full-structure materials. The material *minority carrier lifetimes* were characterized by time-resolved photoluminescence (TRPL). The variation of As and P atoms and impurity *concentration* with *thickness* at the material structure interface were gauged by SIMS. The fluctuation of the $In_{0.53}Ga_{0.47}As$/InP heterojunction interface and necessary geometrical information is observed by scanning transmission electron microscopy (STEM). Finally, planar APD devices were prepared, and the *IV* characteristics were measured.

The effect of As-source deoxidation conditions is superior to that of P-source deoxidation conditions in terms of material surface morphology, lattice quality, *minority carrier lifetime*, and *dark device current*. This work offers a practical foundation for identifying optimal epitaxial growth and device processing parameters for InP-based InGaAs/InP.

1 Experiments

1.1 Material growth

The left side of Figure 1 shows the InGaAs/InP APD device structure cross-section, and the right shows the electric field distribution. To evaluate the effect of different deoxidation atmosphere conditions of As_4 and P_2 on the APD device performance, we grew high-quality InGaAs/InP APD epitaxial materials on AXT (100) InP substrates using the MBE (DCA P600) system. A three-temperature valve-controlled solid-state phosphorus cracking source and a two-temperature valve-controlled arsenic cracking furnace were used as the group V sources, and conventional Knudsen cells for Gallium and Indium are used as the group III source.

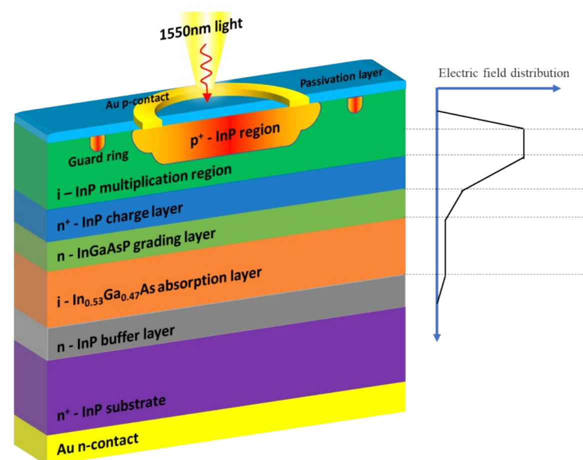

Fig. 1 Profile diagram and internal electric field distribution of InGaAs/InP APD structure

图1 InGaAs/InP APD结构的剖面图和内部电场分布

The InP substrate was first put into the load lock and baked at 200°C to remove the adsorbed water vapor and then degassed in a pretreatment chamber at 300°C for 20 min. In the growth chamber, the intensity of the beam flux of each source at different *temperatures* was corrected to determine the growth *temperature* of each source. The beam flux ratios of group V and group III elements were determined using the beam flux monitors

（BFM）. The substrate was then transferred to the growth chamber. The substrate *temperature* of sample A was elevated under the protection of the As_4 atmosphere, and sample B was performed under the P_2 atmosphere to desorb the oxides from the surface. A clear 2×4 reconstitution stripe appeared on the reflection high-energy electron diffraction（RHEED）fluorescence screen, indicating desorption of the oxide layer on the substrate surface[9]. Afterward, the sample holder temperature continued to be raised by 30° C（thermocouple *temperature* ~ 640°C）and maintained for 6-7 min to allow complete desorption of the oxide film and flattening of the atomic layer on the substrate surface. After cooling down to the growth *temperature*, the beam equivalent pressure（BEP）ratios of each beam source furnace were controlled by valves to epitaxially grow 1~2 μm lattice-matched unintentionally doped $In_{0.53}Ga_{0.47}As$/InP film materials, and APD structured wafers. The APD material was based on a separate absorption, grading, charge, and multiplication（SAGCM）structure, including an n-InP buffer layer, an intrinsic $In_{0.53}Ga_{0.47}As$ absorber layer, an InGaAsP component gradient layer, an n-type highly doped InP charge control layer, intrinsic InP cap layer, divides into Sample A（As_4 deoxygenated）and Sample B（P_2 deoxygenated）[4].

1.2 Material characterization

After growth, the materials were characterized using XRD to determine the component values and the lattice quality. Van der Pauw method Hall test（Ecopia HMS-3000）was performed to characterize the carrier transport properties of epitaxial $In_{0.53}Ga_{0.47}As$/InP materials of different thicknesses.

TRPL can characterize the direct electron-hole recombination（band-to-band recombination）, Shockley-Read-Hall（SRH）recombination, and other non-radiative recombination information of materials absorbing pulsed laser radiation. [12]. The time-correlated single-photon counting（TCSPC）is a crucial technique for fluorescence *lifetime* imaging due to its high signal-to-noise ratio and high temporal resolution[13]. The dynamics of carrier recombination in APD structure materials were studied using the TCSPC method with a 1064 nm laser, and the results were compared with samples from the anti-reflective coating（ARC）SiNx passivation treatment（front-end process）[14]. The single-photon detector is a Hamamatsu H10330C -75 microchannel plate detector with a time resolution of 20 ps.

The SIMS principle is to use a focused ion beam sputtering the surface of semiconductors and then use a time-of-flight or mass spectrometer to analyze the secondary ions formed in the sputtering process, which allows for high-precision detection of the elemental distribution and interface impurities in the film materials from nanometer to tens of microns in depth[15, 16]. We used the SIMS（Cameca IMF 5F, Evans Analytical Group）test to observe the high-precision measurement of different elemental *concentrations* in structural samples to analyze and determine the growth behavior and quality of InGaAs lattice epitaxy on InP substrates. *The detection limit (DL)* is over 1.0×10^{10} to 1×10^{16} atoms/cm^{-3}.

Interfaces and defects in MBE-grown InGaAs/InP films were further examined using aberration-corrected STEM. Cross sections of STEM sample A（As_4 deoxygenated）and sample B（P_2 deoxygenated）were prepared using the focused ion beam（FIB）technique（Helios-G4-CX, Thermo Fisher Scientific）. The STEM investigations were performed with a field-emission STEM（Themis Z, Thermo Fisher Scientific）fit with a probe and an image aberration corrector（SCORR and CETCOR, CEOS GmbH）. The microscope was operated at 300 kV. For HAADF-STEM imaging, the probe semi-convergent *angle* was set to 21.4 mrad, and the semi-collection *angle* of the detector was arranged from 76 to 200 mrad. The STEM images were collected with［101］zone axis.

1.3 Device preparation and characterization

After characterization, the incident surfaces of APD materials were coated with SiNx ARC to eliminate reflections from the air-InP interface. The wafers were fabricated into 20 μm diameter planar InGaAs/InP APD by front-end processes such as Zn doping and UV lithography, including Device A（As_4 deoxygenated）and Device B（P_2 deoxygenated）[11, 17]. The *IV* characteristics were measured by a semiconductor parameter analyzer（Keysight 4200）at room *temperature*.

2 Results and discussions

2.1 Hall effect analysis

Figure 2 shows *the carrier concentration n* and *Hall mobility* μ of epitaxially grown unintentionally doped $In_{0.53}Ga_{0.47}As$/InP films under different deoxidation atmospheres at 330K and 77K. Four samples exhibit lower *carrier concentrations* at 77K than 300K. In contrast, *μ values* at 77K are higher than that at 300K, with *mobility* even exceeding $6.0\times10^4 cm^2/Vs$. This is due to the decreased lattice vibration scattering caused by low *temperatures*（$\mu_{phonon} \propto T^{-3/2}$）, fewer impurity scattering noises from the $In_{0.53}Ga_{0.47}As$ intrinsic growth（$\mu_{lattice} \propto T^{3/2}$）, and lower transport energy of the thermally activated carriers. Thus, the $In_{0.53}Ga_{0.47}As$/InP materials with As_4 protective atmosphere possess superior carrier transport capability than those with P_2 deoxidation protection, with higher mobility and lower carrier concentration. This suggests that As_4 deoxidation can help reduce impurity contamination and associated point defects introduced by the growth process.

2.2 TRPL analysis

Figure 3 shows the time instrumental response function（IRF）fluorescence decay curves generated and extracted under a single laser pulse for the TRPL test. For the APD structured wafer, the 1064 nm light pulse is mainly absorbed by the InGaAs layer, and *the minority carrier lifetime* is reflected in the InGaAs layer. It is generally believed that the InP cap layer has little impact on the absorption layer of the 1064 nm light[10]. The double exponential fit（ExpDec2）using the nonlinear least squares inverse convolution method is set to obtain *the minority carrier lifetimes t1* and *t2*, which generally correspond to the SRH recombination *t1*（*shorter lifetime*）and

radiation recombination *t2* (*longer lifetime*) of the InP charge layer or InGaAs layer of the APD materials. Although the model presents several limitations and drawbacks, it is accepted due to its simplicity [18].

The smoother the decay of the measured TRPL curve, the larger *the τ value*, indicating the stability of wafer quality. The smaller the variation of *the τ value*, the better the wafer quality. We can see that As_4 deoxidation has a longer *minority carrier lifetime t2* than P_2 deoxidation, indicating that the wafer of As_4 deoxidation is of better quality than that of P_2 deoxidation, with relatively fewer lattice defects and impurities and less radiation recombination. *The t1* of the samples is tiny, which indicates that the carriers in the wafer are rapidly quenched after capture, with strong non-radiative recombination, and there may be many deep energy level recombination with high doping *concentrations* or background *concentrations*.

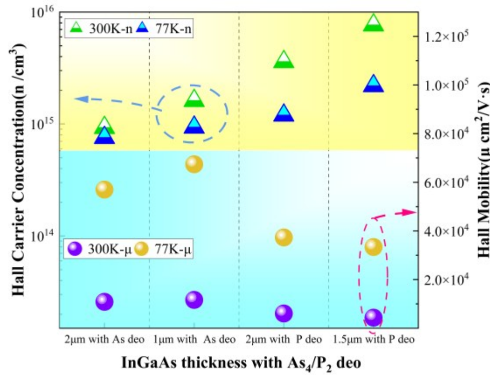

Fig. 2 Hall carrier concentration and mobility plot
图2 霍尔载流子浓度和迁移率图

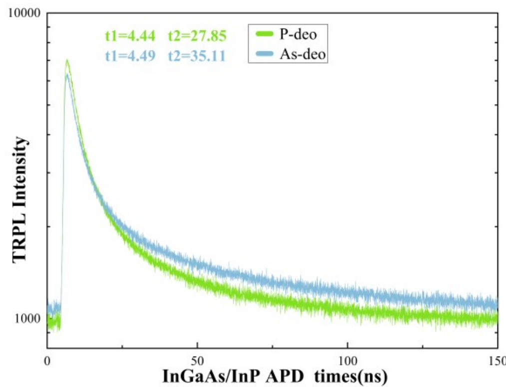

Fig. 3 TRPL spectra of APD wafers
图3 APD晶圆的TRPL光谱

2.3 SIMS analysis

Figure 4 (a) shows *the depth* distribution of Ga, As, P, In (right axis) and O, C, H, N, Si (left axis) in the MBE-grown InGaAs/InP APD wafers. The near-surface trailing in the SIMS profiles, especially for C, O, and H, can be explained by the kick-on of the impurity atoms from the surface contaminations into *the depth* by the primary ion beam and no more than 20-50 nm[19]. Different deoxidation conditions do not distinctly affect *the concentrations* of Ga and P, As, and In of sample A (As_4 deoxidation) and sample B (P_2 deoxidation). However, O and Si impurities increased when switching the valve sources for GaAs and InP growth (d = 2-3μm, d = 4.8-5.6μm). C and H content increase significantly at deoxidation (d = 4.8-5.6μm). In Figure 4 (b), the increase in O content at d = 4.8-5.6μm is more significant for sample B than sample A. This tailing could represent impurity concentration in the matrix, or it may be caused by impurity segregation at grain boundaries and dislocations and secondary implantation of the surface contaminants. Therefore, we perform a retest to avoid the interference caused by the surface contaminants. Table 1 summarizes the peak results of the two SIMS tests for C, O, N, H, and Si impurities, with no change in the data values. However, sample B has an O *concentration* nearly an order of magnitude higher than A, despite being close to *the detection limit*. This implies that P_2 deoxidation during MBE may have more negative effects than As_4 deoxidation, which may cause impurity accumulation on the rough surface, lattice, and interfacial dislocations of the material[19].

2.4 STEM analysis

Figure 5-6 shows the HAADF-STEM images of the epitaxial cross-sectional structure of sample A (As_4 deoxidation) and sample B (P_2 deoxidation). According to the Z-contrast imaging mechanism of HAADF-STEM, the elements of Ga, and As shown brighter contrast than P atoms, giving InP, InGaAsP, and InGaAs their distinct differences in atomic resolved images[20]. Figures 5 (a) and 6 (a) show the wafer epitaxial cross-sectional structure. Figures 5 (b) and 6 (b) show a detailed scan of the InP buffer layer and InGaAs absorber layer heterojunction interface. Figures 5 (c) and 6 (c) show the InP buffer and substrate homojunction interface. Sample A clearly shows the sharp and straight interface between InGaAs and InP buffer layer and InP substrate, which is atomically smooth. Sample B shows only a slightly floating heterogeneous interface. And the homogeneous interface could not be characterized with grayscale fluctuations. Stacked layer dislocations or lattice distortions may lead to interface roughness[20,21]. This indicates that

Table 1 Average peak concentrations (cm^{-3}) of impurities in bulk regions (d = 4.8–5.6 μm) from SIMS measurements.
表1 SIMS测量的(d = 4.8–5.6μm)的区域杂质平均最大浓度(cm−3)

Sample	O	C	H	Si	N
A	2.25E+17	9.76E+18	2.08E+18	1.56E+17	1.86E+16
B	8E+17	9.09E+18	1.34E+18	3.74E+17	6.61E+16
DL	1E15	1E15	1E16	1E14	5E14

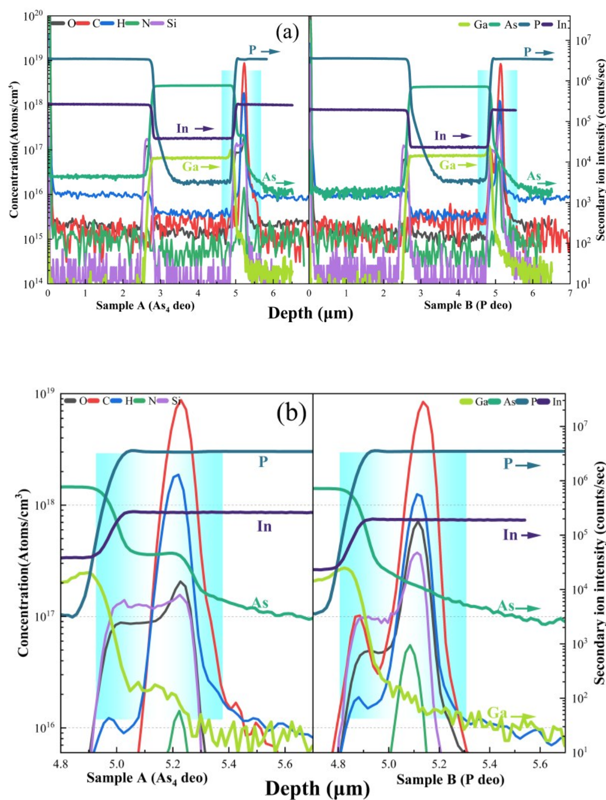

Fig. 4　(a) Comparison of SIMS depth distributions for Samples via As_4, P_2 deoxidation, (b) Bulk regions (d = 4.8-5.6 μm) of comparison of deoxidation interface

图4　(a) 通过As4、P2脱氧样品的SIMS深度分布对比，(b)深度d = 4.8-5.6 μm的脱氧界面对比

sample A has a more explicit interface and better interfacial quality than sample B.

As shown in Fig. 5(d) and Fig. 6(d), the InGaAs layer appears as dumbbells at the atomic-scale resolution, InP appear as single dots, and the interfacial atomic layers are regularly arranged[22]. It indicates that the initial growth of MBE under As_4 deoxidation conditions is controlled precisely, and the InP buffer layer can be stably controlled at the atomic scale. However, the unevenness of the heterogeneous interfaces of Sample B causes some heterojunctions to be identified in atomic resolution hardly. Therefore, the As_4 deoxidation process avoids more defects and improves the lattice quality. This may be because As atoms are more challenging to stay on the substrate surface than P atoms. Sufficient or excess As_4 sources can ensure adequate absorption of impurities such as oxygen of the substrate surface by reducing the In-O bonding on the surface while avoiding the metallization of the As atoms on the InAs surface by desorption[23-25].

2.5　Device IV analysis

Figure 7(a) shows the *current–voltage* (*IV*) characteristics of InGaAs/InP APD Device A (As_4 deoxidation) and Device B (P_2 deoxidation) operating in linear mode. Based on the collisional ionization principle of phonon

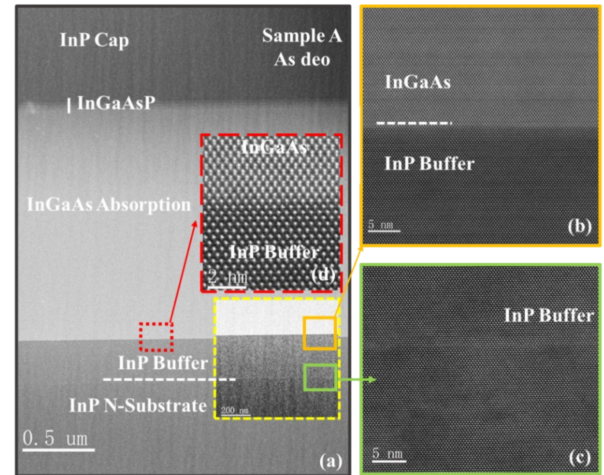

Fig. 5　STEM-HAADF image of APD sample A (As-deoxidation) (a) an image of the APD structure on FIB grid, (b) the image of InGaAs and InP buffer, (c) zoom region of InP homojunction interfaces, (d) high-resolution images of the region marked with a red frame in (a)

图5　APD样品A的STEM-HAADF图像(As-脱氧)(a)FIB网格上的APD结构图像，(b)InGaAs和InP缓冲层的图像，(c)InP同质结界面的区域，(d)(a)中红框区域的高分辨率图像

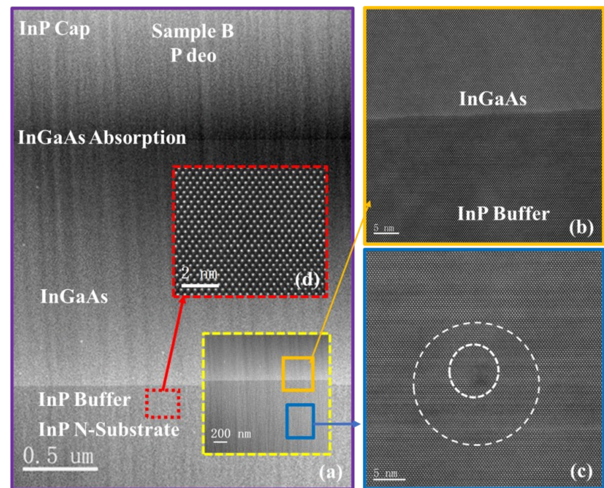

Fig. 6　STEM-HAADF image of APD sample B (P-deoxidation) (a) an image of the APD structure on the FIB grid, (b) the image of InGaAs and InP buffer, (c) the zoom region of InP homojunction interfaces and stacking fault (circled). Circles indicate dislocations with different core structures, (d) high-resolution images of the area marked with a red frame in (a)

图6　APD样品B的STEM-HAADF图像(P-脱氧)(a) FIB网格上的APD结构图像，(b)InGaAs和InP缓冲层的图像，(c)InP同质结界面的区域和堆叠缺陷(圆圈)圆圈表示具有不同核心结构的位错，(d)(a)中红框区域的高分辨率图像

scattering, the hot carriers in the InP collide with the lattice to generate *dark current* and zero *photocurrents* at lower *reverse bias voltages*. When the APD reaches *the punch through voltage* (near 15 V), the depletion region extends to the InGaAs absorption region. When *the reverse bias voltage* is between 15V and 60V, electrons move toward the substrate and holes toward the InGaAsP grading layer and the InP multiplication layer. At the same time, the number of carriers in collisional ionization increases

until *the breakdown voltage* (near 60 V) is reached, *the current* is wholly transferred to the multiplication layer, and the APD enters the Geiger mode from the linear mode[26-28]. The main components of *dark current* include *the generation-recombination current, tunneling current, and leakage current. Generation-recombination current* is affected by *carrier concentrations, minority carrier effective lifetime* τ_{eff} and *temperature. Tunneling current* is mainly affected by *band gap* and *trap energy levels*. Higher *carrier mobility* and a longer *lifetime* can usually reduce *the dark current* of the device. Considering that surface leakage and weak external natural light interference have little effect on device applications, we ignore the differences in *the dark current* below *the punch-through voltage* [11, 29].

Compared to device A (As_4 deoxidation), device B (P_2 deoxidation) has a lower *punch-through voltage*, a slightly higher *breakdown voltage*, and a more extended linear region (less than 1 V). This is mainly due to the small *thickness* difference of the InP multiplication layer[28, 30]. *The elevated bias voltage* increases *the tunneling current* in the absorption layer, which can lead to a significant increase in *the dark current*, thus affecting the performance and power consumption of the device. We note that near *the punch-through voltage*, *the dark current* of device B is 2.62×10^{-9} A, an order of magnitude larger than *the dark current* of device A of 1.62×10^{-10} A. From figure 2, *the carrier concentration* of the InGaAs layer with As_4 deoxidation is lower, thus resulting in a lower *dark current* at *the punch-through voltage*. Meanwhile, the higher *carrier mobility* of InGaAs layers implies fewer intrinsic defects in the As_4 deoxidation materials. Therefore, *the generation-recombination current* caused by defects is relatively small.

The carrier lifetime measured for wafers is not *the bulk carrier lifetime* τ_b but rather *the effective lifetime* $\tau_{eff} \leq \tau_b$, including surface and bulk recombination. When the surface layer of the wafer is coated with SiNx passivation, it can reduce the surface recombination and reflection loss, enhance the absorption of light, and suppress *the surface leakage*, which makes τ_{eff} closer to τ_b [31, 32]. Figure 7(b) shows the TRPL curves of APD wafers after ARC. Both *t1* and *t2* increase significantly, and *the effective lifetime* with As_4 deoxidation τ_{eff} is longer than that with P_2 deoxidation. This indicates that ARC has improved the performance of APD, but As_4 deoxidation still maintains better performance than P_2 deoxidation.

Combined the *IV* analysis with the above Hall test and TRPL results, the APD with As_4 deoxidation has lower *carrier concentrations*, higher *Hall mobilities*, and higher *minority carrier lifetimes* compared to the P_2 deoxidation, which produces some suppression of the *dark current* caused by point defects or impurity defect *energy levels*. The SIMS and STEM results also support this view further.

3 Conclusions

In summary, we used the MBE technique to deoxidize InP substrates under As_4 and P_2 atmosphere protection and grow $In_{0.53}Ga_{0.47}As$/InP epitaxial layer APD structures. The material quality is evaluated by STEM, TRPL, Hall test, SIMS, and other characterization methods. The APD devices were prepared by a front-end process. The *IV* characteristics were measured at room *temperature*. The effects of MBE deoxidation conditions on the material surface morphology, lattice quality, *minority carrier lifetime*, and *dark device current* were analyzed. The results show that compared with P_2 deoxidation, As_4 deoxidation can significantly improve the MBE material quality, make the heterogeneous interface structure stable and sharp, improve *the Hall mobility*, reduce *the carrier concentration*, lengthen *the minority carrier lifetime*, and have a specific suppression effect on *the device dark current* caused by point defects or impurity defects. This study provides valuable information on InP/InGaAs APD material devices prepared by MBE.

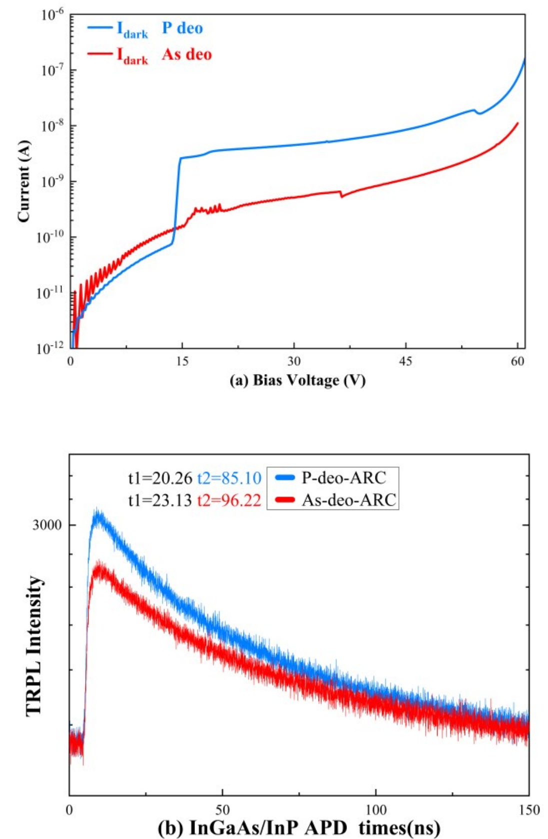

Fig. 7 (a) *I-V* and gain characteristics of the InGaAs/InP APD, (b) TRPL spectra of ARC-APD

图7 (a)InGaAs/InP APD的I-V曲线,(b)经钝化处理的APD材料TRPL光谱

References

[1] LI Xue, GONG Hai-Mei, SHAO Xiu-Mei, *et al*. Recent advances in short wavelength infrared InGaAs focal plane arrays[J]. J. Infrared Millim. Waves, 2022, **41**(1): 129-138(李雪,龚海梅,邵秀梅,等. 短波红外InGaAs焦平面研究进展[J]. 红外与毫米波学报), 2022, **41**(1): 129-138.

[2] NAMEKATA N, MAKINO Y, INOUE S. Single-photon detector for long-distance fiber-optic quantum key distribution [J]. *Optics Let-*

ters, 2002, **27**(11): 954-6.

[3] MENDENHALL J A, CANDELL L M, HOPMAN P I, *et al*. Design of an Optical Photon Counting Array Receiver System for Deep-Space Communications [J]. *Proceedings of the IEEE*, 2007, **95** (10): 2059-69.

[4] JIANG X, WILTON S, KUDRYASHOV I, *et al*. InGaAsP/InP Geiger-mode APD-based LiDAR [M]. Optical Sensing, Imaging, and Photon Counting: From X-Rays to THz. 2018.

[5] LEWIS J S, LEO G, BROWN G J, *et al*. Development of an InGaAs SPAD 2D array for flash LIDAR [M]. Quantum Sensing and Nano Electronics and Photonics XV. 2018.

[6] PANISH M B. Molecular Beam Epitaxy of GaAs and InP with Gas Sources for As and P [J]. *Journal of The Electrochemical Society*, 1980, **127**(12): 2729-33.

[7] YANG Ying, WANG Hong-Zhen, FAN Liu-Yan, *et al*. Study on Molecular Beam Epitaxy of High indium InGaAs Films[J]. J. Infrared Millim. Waves, 2022, **41**(6): 987-994(杨瑛,王红真,范柳燕、等.分子束外延高铟组分InGaAs薄膜研究[J].**红外与毫米波学报**),2022,**41**(6):987-994

[8] BASTIMAN F, CULLIS A G. GaAs(001) planarization after conventional oxide removal utilising self-governed InAs QD site selection [J]. *Applied Surface Science*, 2010, **256**(13): 4269-71.

[9] KHAIREH-WALIEH A, ARNOULT A, PLISSARD S, *et al*. Monitoring MBE Substrate Deoxidation via RHEED Image-Sequence Analysis by Deep Learning [J]. *Crystal Growth & Design*, 2023, **23** (2): 892-8.

[10] ZHANG Y, GU Y, ZHENG W, *et al*. Anomalous arsenic diffusion at InGaAs/InP interface [J]. *Materials Research Express*, 2018, **6**(3):

[11] GUO Z, WANG W, LI Y, *et al*. Material Defects and Dark Currents in InGaAs/InP Avalanche Photodiode Devices [J]. *IEEE Transactions on Electron Devices*, 2022, 1-6.

[12] AHRENKIEL R K, ELLINGSON R, JOHNSTON S, *et al*. Recombination lifetime of In0.53Ga0.47As as a function of doping density [J]. *Appl Phys Lett*, 1998, **72**(26): 3470-2.

[13] XIAO D, SAPERMSAP N, SAFAR M, *et al*. On Synthetic Instrument Response Functions of Time-Correlated Single-Photon Counting Based Fluorescence Lifetime Imaging Analysis [J]. *Frontiers in Physics*, 2021, **9**

[14] ROSFJORD K M, YANG J K W, DAULER E A, *et al*. Nanowire Single-photon detector with an integrated optical cavity and anti-reflection coating [J]. *Opt Express*, 2006, **14**(2): 527-34.

[15] EBNESAJJAD S. Chapter 4 - Surface and Material Characterization Techniques [M]//EBNESAJJAD S. Surface Treatment of Materials for Adhesive Bonding (Second Edition). Oxford; William Andrew Publishing. 2014: 39-75.

[16] IYENGAR V V, NAYAK B K, GUPTA M C. Silicon PV devices based on a single step for doping, anti-reflection and surface passivation [J]. *Solar Energy Materials and Solar Cells*, 2010, **94**(12): 2205-11.

[17] WEN J, WANG W J, CHEN X R, *et al*. Origin of large dark current increase in InGaAs/InP avalanche photodiode [J]. *Journal of Applied Physics*, 2018, **123**(16):

[18] PéAN E V, DIMITROV S, DE CASTRO C S, *et al*. Interpreting time-resolved photoluminescence of perovskite materials [J]. *Physical Chemistry Chemical Physics*, 2020, **22**(48): 28345-58.

[19] RESHCHIKOV M A, VOROBIOV M, ANDRIEIEV O, *et al*. Determination of the concentration of impurities in GaN from photoluminescence and secondary-ion mass spectrometry [J]. *Scientific Reports*, 2020, **10**(1): 2223.

[20] SMITH D J. Atomic-resolution structure imaging of defects and interfaces in compound semiconductors [J]. *Progress in Crystal Growth and Characterization of Materials*, 2020, **66**(4): 100498.

[21] PAULAUSKAS T, BUURMA C, COLEGROVE E, *et al*. Atomic scale study of polar Lomer - Cottrell and Hirth lock dislocation cores in CdTe [J]. *Acta Crystallographica Section A*, 2014, **70**(6): 524-31.

[22] CHU M W, LIOU S C, CHANG C P, *et al*. Emergent Chemical Mapping at Atomic-Column Resolution by Energy-Dispersive X-Ray Spectroscopy in an Aberration-Corrected Electron Microscope [J]. *Physical Review Letters*, 2010, **104**(19): 196101.

[23] SCHäFER M, NAUMANN W, FINNBERG T, *et al*. UV/ozone-activated growth of oxide layers on InAs(001) surfaces and oxide desorption under arsenic pressure [J]. *Applied Surface Science*, 2000, **158** (1): 147-58.

[24] ZHOU X, LUO Z-J, GUO X, *et al*. Surface segregation of InGaAs films by the evolution of reflection high-energy electron diffraction patterns [J]. *Chinese Physics B*, 2012, **21**(4):

[25] NAOKI KOBAYASHI N K, YASUYUKI KOBAYASHI Y K. As and P Desorption from III-V Semiconductor Surface in Metalorganic Chemical Vapor Deposition Studied by Surface Photo-Absorption [J]. *Japanese Journal of Applied Physics*, 1991, **30**(10A): L1699.

[26] ZENG Q Y, WANG W J, WEN J, *et al*. Dependence of dark current on carrier lifetime for InGaAs/InP avalanche photodiodes [J]. *Optical and Quantum Electronics*, 2015, **47**(7): 1671-7.

[27] MOHAMMADNEJAD S, AGHAEI F. Noise characteristics improvement of submicron InP/InGaAs avalanche photodiode for laser detection system [J]. *Opt Commun*, 2020, 455124561.

[28] LI K, DUAN X, LIU K, *et al*. High-speed and low dark current InGaAs/InAlAs avalanche photodiodes with P-type absorption layers [J]. *Optical and Quantum Electronics*, 2023, **55**(5): 422.

[29] ZENG Q Y, WANG W J, WEN J, *et al*. Effect of surface charge on the dark current of InGaAs/InP avalanche photodiodes [J]. *Journal of Applied Physics*, 2014, **115**(16): 164512.

[30] XU J, CHEN X, WANG W, *et al*. Extracting dark current components and characteristics parameters for InGaAs/InP avalanche photodiodes [J]. *Infrared Physics & Technology*, 2016, 76(468-73.

[31] SCHMIDT J, ABERLE A G. Easy-to-use surface passivation technique for bulk carrier lifetime measurements on silicon wafers [J]. *Progress in Photovoltaics*: *Research and Applications*, 1998, **6**(4): 259-63.

[32] POLLOCK K L, JUNGE J, HAHN G. Detailed Investigation of Surface Passivation Methods for Lifetime Measurements on P-Type Silicon Wafers [J]. *IEEE Journal of Photovoltaics*, 2012, **2**(1): 1-6.